International Journal for Housing Science and Its Applications
Publish August 10, 2025. Volume 46, Issue 4 Pages 6190-6206

https://doi.org/10.70517/ijhsa464454

Innovation in Distribution Automation Technology through the Integration of Smart Grids and the Internet of Things

Jianjun Zhu[1,*], Gang Wang[2], Qingyun Chen[1], Yafei Huang[1] and Wen Yang[2]
[1] State Grid Gansu Electric Power Company, Lanzhou, Gansu, 730000, China
[2] Gansu Tongxing Intelligent Technology Development Co., LTD., Lanzhou, Gansu, 730000, China
Corresponding authors: (e-mail: zhujj1069@163.com).

Abstract In view of the current problems of insufficient communication technology and real-time performance, and weak data processing and analysis capabilities, this paper proposes a technical solution that integrates the Internet of Things (IoT) and the improved 5G-TSN (Time-Sensitive Networking) model to improve the real-time control capabilities of the smart grid by integrating the Internet of Things technology. The model relies on the ubiquitous perception capability of the Internet of Things to achieve a full life cycle management of devices. Firstly, a multi-dimensional sensor network is constructed at the perception layer; the FlexE (Flexible Ethernet) interface is used to implement hard-isolated network slicing; the IEEE 802.1AS time synchronization protocol is deployed. Secondly, an edge computing gateway with AI (artificial intelligence) inference capabilities is deployed in the ring network cabinet, and a containerized microservice architecture based on Kubernetes is constructed to achieve intelligent collaborative management and control of Internet of Things devices. Then, a digital twin of the feeder automation device is established; an electromagnetic transient model is constructed using the Modelica language; a real-time data interaction interface based on OPC UA (Open Platform Communications Unified Architecture) is developed to open up the Internet of Things channel between physical devices and digital twins. Finally, the distribution automation performance is verified. Experiments show that the end-to-end latency is only about 8ms in normal load scenarios and about 22ms in encrypted transmission scenarios. The improved 5G-TSN model keeps the processing latency at a low level in most scenarios, and the accuracy rate reaches more than 95% within 3 seconds in single-phase grounding fault scenarios. The improved method can solve the problems of communication technology and real-time performance while improving data processing and analysis capabilities. This research provides technical support for building a highly elastic and adaptive new power system. Its cross-domain fusion paradigm can be extended to multiple scenarios of the energy Internet, which has significant economic value and social benefits in promoting the digital transformation of the power system.

Index Terms Smart Grid, Internet of Things Technology, Distribution Automation, 5G-TSN Model, Digital Twin

I. Introduction

Driven by the global energy structure transformation and the “dual carbon” goal, smart grids, as the core carrier of new power systems [1], are accelerating their evolution towards digitalization and intelligence [2], [3]. As the hub link between the transmission network and end users [4], the operating efficiency of the distribution automation system directly affects the reliability of power supply and the level of energy utilization [5], [6]. However, the current distribution field faces two major technical bottlenecks. On the one hand, traditional optical fiber communications and wireless networks are difficult to meet the low latency requirements of new loads such as distributed energy access and electric vehicle charging piles in high-concurrency scenarios, resulting in fault response latency [7], [8]. On the other hand, the massive heterogeneous data such as PMU (phasor measurement unit) data, device status parameters, and user power consumption information generated by distribution terminal devices have the phenomenon of “data islands” [9], [10]. The existing data processing architecture is limited by the centralized cloud computing model [11], resulting in excessive fault diagnosis latency and difficulty in supporting the rapid self-healing needs of the power grid [12]. The superposition effect of these problems exposes the vulnerability of the existing technical system in extreme scenarios. In this context, exploring the deep integration path of IoT technology and smart grid and building a distribution automation system with real-time perception, dynamic optimization, and autonomous decision capabilities [13], [14] have become the key to promoting the construction of new power systems. This technology integration provides distribution automation with ubiquitous perception, multi-dimensional data integration, and device life cycle management capabilities. Its cross-domain integration

paradigm can be extended to multiple scenarios of the energy Internet, which has significant economic value and social benefits in promoting the digital transformation of power systems.

In response to the above challenges, the academic community has carried out multi-dimensional technical research. Butt O M [15] et al. improved the reliability, efficiency, and sustainability of the distribution system by integrating IoT and smart grid technologies. However, the lack of real-time performance of traditional communication architecture [16] and the data island problem caused by centralized cloud computing still restrict system performance [17]. Through phase-splitting switch and fault identification technology [18], [19], Zhang W [20] et al. proposed a fault location and isolation method based on adaptive reclosing [21], which solved the problems of secondary impact and long power outage time of the traditional voltage-time scheme, but did not involve the coordinated optimization of IoT communication and edge computing, and still had insufficient adaptability when dealing with dynamic topological changes of distributed energy access. Ghiasi M [22] et al., by constructing a mathematical model of the integration of IoE (Internet of Energy) and smart grid [23], revealed the role of distributed energy integration in promoting carbon emission reduction [24]. However, there is still a gap in the research on energy mismatch and implicit carbon emissions caused by Internet technology. Although these studies have made phased progress, they generally have the limitations of “local optimization and global fragmentation”, which makes it difficult to meet the comprehensive requirements of new power systems for real-time communication, data integration, and control coordination.

To break through the boundaries of existing technologies, some scholars have begun to explore cross-domain technology integration paths. Orlando M [25] et al. proposed a distributed smart meter architecture based on the Internet of Things. By integrating two-way communication, self-configuration algorithms, and dynamic update functions [26]-[28], they solved the problems of fixed functions and poor scalability of traditional smart meters and verified the feasibility of low-cost hardware implementation. However, this solution does not involve the real-time optimization mechanism of communication in high-concurrency scenarios, and the security protection system lacks the support of national secret algorithms, which makes it difficult to meet the needs of new power systems for multi-service isolation and encryption latency collaborative control. By integrating Wi-Fi/RS-485 communication and Modbus protocol [29], Sheba M A [30] et al. proposed a low-cost IoT RTU (Remote Terminal Unit) solution based on microcontrollers [31], which solved the problems of poor compatibility and high upgrade costs of traditional power grid devices. However, its microcontroller architecture still has computing power bottlenecks in real-time data processing and complex AI (artificial intelligence) inference scenarios, and does not involve the deterministic latency guarantee mechanism of time-sensitive networking (TSN). Zhou B [32] et al. reviewed the architecture design and control strategy of MMGEMS (Multi-Microgrid Energy Management Systems) and proposed an information-physical collaboration method based on clustered energy scheduling [33], which solved the energy efficiency optimization and elasticity improvement problems in distributed energy access scenarios. However, there are still technical bottlenecks in the real-time guarantee of the decentralized communication architecture of the system and the coordinated control of multiple microgrids in extreme scenarios. These research trends indicate that through the deep integration of 5G-TSN heterogeneous networks and the native integration of edge computing and AI algorithms, a four-dimensional collaborative technology system of perception-communication-computing-control can be built to systematically solve the core contradictions in the development of distribution automation.

Based on the above analysis, this study aims to establish a new distribution automation paradigm that integrates smart grid and IoT technology. The specific innovation is reflected in three dimensions. A 5G-TSN hybrid scheduling algorithm based on dynamic weight allocation is proposed. By integrating network calculation and reinforcement learning technology, a dynamic optimization model of multi-dimensional QoS (Quality of Service) parameters (latency, jitter, bandwidth) is constructed. A lightweight space-time graph convolutional network (ST-GCN) for edge devices is developed, and the model parameter volume is compressed to 0.8MB through knowledge distillation technology. Finally, a distribution automation verification platform based on digital twins is constructed, integrating the RT-LAB (Real-Time Laboratory) real-time simulation system and the IoT device simulation cluster to complete the full process verification of fault location, isolation, and power supply restoration. From the perspective of large-scale application, the fusion architecture proposed in this study is not only suitable for typical scenarios such as rural power grid transformation and industrial park energy management, but can also be extended to emerging fields such as urban rail transit and port shore power through technical adaptability optimization, and reserves interfaces for the future 6G communication and quantum encryption technology power scene integration, showing the technical vitality of sustainable iteration.

II. IoT and 5G-TSN Converged Architecture Design

II. A.2.1 Optimized Design of 5G-TSN Communication Architecture

In response to the technical challenges of differentiated latency requirements for multiple services in distribution automation systems, this study uses FlexE interfaces to implement physical layer network slicing. Through SPN (Slicing Packet Network) device deployment, the 100Gbps physical link is divided into three independent sub-interfaces: control service, protection service, and monitoring service. The control service sub-interface is configured with 25Gbps bandwidth and a time slot allocation granularity of 5Gbps. The protection service sub-interface is configured with 50Gbps bandwidth and a time slot granularity of 10Gbps. The monitoring service sub-interface is configured with 25Gbps bandwidth and a time slot granularity of 5Gbps. Each sub-interface is bound to a time slot through the FlexE Calendar mechanism to build a physical layer hard isolation channel to achieve differentiated carrying of control services, protection services, and monitoring services.

In the communication link from the ring main unit to the distribution master station, an industrial Ethernet switch that supports TSN features is deployed, and the IEEE 802.1Qbv gating mechanism is enabled. For the periodic telemetry data of FTU (Feeder Terminal Unit), the 802.1Qbv time window is configured to 200μs, aligned with the 5G air interface TTI (Transmission Time Interval), and latency jitter is eliminated through traffic shaping. For event-driven messages of fault indicators, the IEEE 802.1Qbu frame preemption function is enabled to cut high-priority messages into 64-byte micro-segments to ensure the transmission priority of critical services. The upper limit of the latency of TSN gating scheduling can be quantified and analyzed by the following equation:

$$D_{tsn} \leq \sum_{k=1}^{m} \left(\frac{L_k}{C} + \sum_{j=1}^{n_k} \tau_j \right) + \Delta_{sync} \tag{1}$$

Among them, L_k is the length of the k-th time window; C is the link capacity; τ_j is the frame preemption latency; Δ_{sync} is the clock synchronization error.

The time synchronization system adopts a hierarchical master-slave architecture and deploys the IEEE 802.1AS-2020 protocol to achieve full network time synchronization. A Stratum-2 master clock is deployed in the 110kV substation to distribute time signals to the aggregation switch in the distribution room. The critical path uses transparent clock correction technology to perform hardware-level compensation for the residence time of IEEE 1588v2 messages inside the switch to eliminate the accumulated error of network transmission latency. The bandwidth transfer amount from the monitoring sub-interface to the control sub-interface is dynamically calculated through a reinforcement learning strategy:

$$B_{control}^{new} = B_{control}^{old} + \eta \cdot \frac{\partial \mathcal{L}}{\partial B_{monitor}} \cdot B_{monitor}^{idle} \tag{2}$$

Among them, η is the learning rate, and $\mathcal{L}$ is the QoS loss function. The bandwidth transfer amount from the monitoring sub-interface to the control sub-interface is dynamically adjusted through reinforcement learning.

In view of the latency accumulation problem under the multi-branch topology of the distribution network, a dynamic bandwidth adjustment algorithm is designed. Based on the OpenFlow protocol, the traffic characteristics at each segment switch are collected to construct a QoS matrix for latency-sensitive services. When a branch line fault is detected, the FlexE sub-interface bandwidth reallocation mechanism is triggered through PCEP (Path Computation Element Communication Protocol), and the 802.1Qbv gating list parameters of the TSN switch are adjusted synchronously to prioritize the transmission resources of the fault isolation instruction. Through the dynamic bandwidth adjustment algorithm, the monitoring service sub-interface can reallocate resources to the control service sub-interface. The dynamic bandwidth adjustment algorithm realizes dynamic resource allocation by establishing a multi-dimensional QoS parameter optimization model, and its mathematical expression is:

$$\min_{\mathbf{w}} \sum_{i=1}^{N} \left(\alpha_i \cdot \frac{D_i(\mathbf{w})}{D_i^{max}} + \beta_i \cdot \frac{J_i(\mathbf{w})}{J_i^{max}} + \gamma_i \cdot \frac{B_i(\mathbf{w})}{B_i^{min}} \right) \tag{3}$$

Among them, w is the bandwidth weight vector; D_i, J_i, and B_i represent the latency, jitter, and bandwidth of the i-th type of service, respectively; α_i, β_i, and γi are normalized weight coefficients. After optimization, the bandwidth occupancy rate of the control service is improved while maintaining the stable carrying capacity of the protection service, as shown in Figure 1.

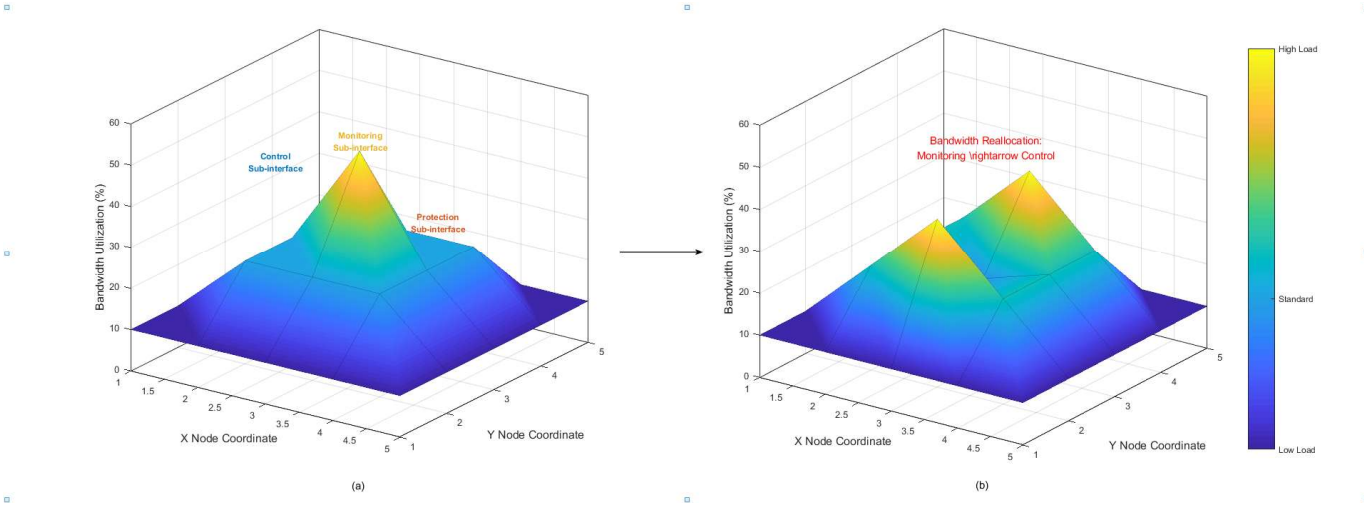

(a) Original network slice resource allocation (b) Optimized network slice resource allocation

Figure 1: Network slice resource allocation optimization

Figure 1 shows the network slice resource allocation optimization solution based on the improved 5G-TSN communication architecture. The original and optimized bandwidth allocation are intuitively presented in the form of a three-dimensional heat map. (a) reflects the bandwidth occupancy distribution of different service sub-interfaces (control, protection, and monitoring) under the traditional static resource allocation strategy, and (b) shows the resource allocation effect after dynamic adjustment, especially how to improve resource utilization in the process of bandwidth redistribution from monitoring services to control services. The load status of each node and its optimization direction are clearly reflected through color mapping and height changes. The marked arrows and text descriptions further emphasize the core idea of the optimization strategy, that is, to achieve flexible resource scheduling under the premise of ensuring low latency and high reliability, so as to meet the real-time requirements of the integration scenario of smart grid and IoT technology.

At the security protection level, the dual isolation mechanism of FlexE sub-interface and IPSec tunnel is adopted. The control service sub-interface enables the AES-256-GCM encryption algorithm; the protection service sub-interface configures the SM4 national encryption algorithm; the monitoring service sub-interface uses the TLS 1.3 (Transport Layer Security) protocol. Through the deep coupling of time-sensitive networks and security protocols, the coordinated optimization of encryption processing and deterministic latency characteristics is achieved.

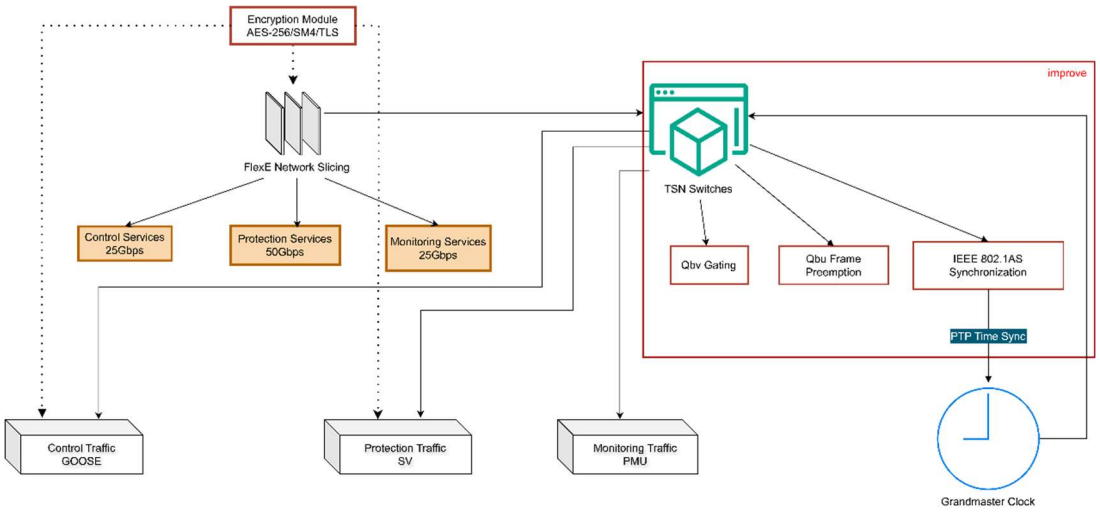

Figure 2: 5G-TSN converged communication architecture

Figure 2 shows the overall design of 5G-TSN converged communication in distribution automation. Physical layer network slicing is achieved through the FlexE interface, and control, protection, and monitoring services are carried on independent hard-isolated sub-interfaces respectively. Combined with the Qbv (IEEE 802.1Qbv) gating and Qbu (IEEE 802.1Qbu) frame preemption mechanism of the TSN switch, low latency and high reliability transmission of multiple service flows are ensured. At the same time, a hierarchical master-slave time synchronization system is adopted to achieve microsecond-level time synchronization of the entire network through the IEEE 802.1AS-2020 protocol and transparent clock correction technology, supplemented by a dynamic bandwidth adjustment algorithm and a dual security encryption mechanism to ensure communication certainty and security in complex distribution network scenarios, and provide a stable and efficient communication foundation for edge computing nodes and digital twin modeling.

II. B.IoT Edge Computing Node Deployment

II. B. 1) Perception Layer Deployment

The perception layer uses heterogeneous sensor networks to achieve holographic perception of distribution devices, and builds a “perception-communication” direct data channel through cross-layer collaborative design of FlexE interface and TSN network. Hall current sensors, fiber optic vibration sensors, and infrared thermal imaging modules are deployed at key nodes of ring network cabinets, and dual-mode networking is achieved through ZigBee 3.0 and LoRaWAN (Long Range Wide Area Network). The multi-protocol adapter based on the FlexE interface realizes the semantic conversion of IEC 61850 and MQTT (Message Queuing Telemetry Transport) protocols. The adapter is linked with the IEEE 802.1Qbv gating mechanism of the TSN switch to dynamically adjust the priority tag of the perception data to ensure that the latency jitter of the GOOSE/SV (Generic Object Oriented Substation Event/Sampled Values) message is $\leqslant$1.5μs. The OPC UA information model is used to uniformly model 12 types of device status parameters (including contact travel, insulation impedance, and partial discharge). Through TSN transparent clock correction technology, the time scale error of the perception data is controlled within 50ns, providing a time and space benchmark for feeder automation. The eBPF (Extended Berkeley Packet Filter) traffic perception module is deployed to implement packet-level extraction of GOOSE/SV message latency jitter characteristics at the XDP (EXpress Data Path) layer. This module is linked with the TSN time-sensitive queue to establish a mapping relationship between the perception data QoS level and the network scheduling strategy.

Table 1: Perception layer sensor selection and performance comparison

Sensor Type	Model/Parameters	Accuracy/Sensitivity	Communication Protocol
Hall Current Sensor	LEM LA 55-P	±0.2%	Modbus RTU
Fiber Optic Vibration Sensor	HBM FS62	0.1 mm/s	CANopen
Infrared Thermal Imaging Module	FLIR A655sc	±1°C	GigE Vision
Partial Discharge Sensor	AE-Sensor PD-300	5 pC Resolution	Ethernet/IP
Temperature-Humidity Sensor	Sensirion SHT35	±0.2°C / ±2% RH	I²C

Table 1 lists in detail the selection and performance parameters of various sensors in the perception layer, including Hall current sensors, fiber optic vibration sensors, infrared thermal imaging modules, partial discharge sensors, and temperature and humidity sensors. These sensors have the characteristics of high precision, high sensitivity, and support for multiple communication protocols, and can realize holographic perception of the operating status of distribution devices, including real-time monitoring of key parameters such as main circuit current, mechanical vibration, device thermal field distribution, insulation status, and ambient temperature and humidity. As a specific embodiment of IoT technology in distribution automation, the perception layer design realizes reliable data transmission through ZigBee 3.0 and LoRaWAN dual-mode networking, and combines the multi-protocol adaptation function of the FlexE interface to uniformly model the collected information and connect it to the upper system, providing ubiquitous perception capabilities for smart grids and supporting the subsequent edge computing, digital twin modeling, and intelligent decision technology.

A hardware parsing module based on Xilinx Kintex-7 FPGA (Field Programmable Gate Array) is developed to realize DMA (Direct Memory Access) direct transmission between IEC 60870-5-104/DNP3.0 protocol messages and GPU memory through AXI (Advanced eXtensible Interface) bus. A zero-copy technology architecture is designed to reduce the COMTRADE fault recording data parsing latency to 5ms, and the GPU acceleration ratio reaches 8.3 times. The GPU acceleration ratio model shows that:

$$S_p = \frac{T_{seq}}{T_{par}} = \frac{N \cdot t_{cpu}}{\frac{N}{P} \cdot t_{gpu} + t_{overhead}} \tag{4}$$

Among them, N is the data volume; p is the number of GPU cores; $t_{overhead}$ is the data transmission overhead. The eBPF traffic perception module is deployed to realize the packet-level extraction of GOOSE/SV message latency jitter characteristics at the XDP layer.

II. B. 2) Edge Computing Architecture

An embedded edge computing gateway is deployed on the ring main unit side. The hardware platform integrates the NVIDIA Jetson AGX Xavier core module and is configured with an 8-core ARM v8.2 CPU and a 512-core Volta GPU architecture. The device is equipped with the Ubuntu 20.04 LTS real-time operating system, and the kernel uses the PREEMPT_RT (Real-Time) patch to optimize the interrupt response characteristics. The dual-redundant 10G network interface card is expanded through the PCIe 3.0 interface to build a dual-active communication link to access the 5G-TSN network. The link is based on the FlexE Calendar mechanism to realize the bandwidth on-demand allocation of the perception data flow and the control instruction flow, and the control service sub-interface bandwidth dynamically adjusts the granularity to realize the parallel transmission of IEC 61850 messages and MQTT protocols. In view of the heterogeneity of the distribution terminal device protocol, a multi-protocol conversion adapter is developed. Xilinx Kintex-7 series FPGA is used to implement hardware parsing modules for protocols such as IEC 60870-5-104, DNP3.0, and Modbus TCP (Transmission Control Protocol), and the protocol data is directly mapped to the GPU memory space through the AXI bus. A parallel decoding pipeline based on CUDA (Compute Unified Device Architecture) is designed to extract time domain features of COMTRADE format fault recording data, and zero-copy technology is used to achieve DMA data transmission between FPGA and GPU.

Containerized microservice architecture is constructed, and K3s lightweight container orchestration system is used for node management. The data acquisition service uses DPDK (Intel Data Plane Development Kit) technology to achieve DMA direct transmission between IEC 60870-5-104/DNP3.0 protocol messages and GPU memory, reducing communication latency. Three types of core microservices are deployed on each edge computing node: the data acquisition service uses DPDK technology to achieve zero packet loss capture of 104 protocol messages. The AI inference service integrates the TensorRT 8.4 optimization engine and supports dynamic loading of ONNX (Open Neural Network Exchange) format models. The engine works with the TSN preemption mechanism to ensure that a high fault identification accuracy rate can be maintained in high electromagnetic interference scenarios such as arc faults. The control decision service uses ROS 2 real-time middleware to achieve millisecond-level response of GOOSE messages. The Kustomize tool is used to achieve differentiated configuration management of different ring network cabinet topologies.

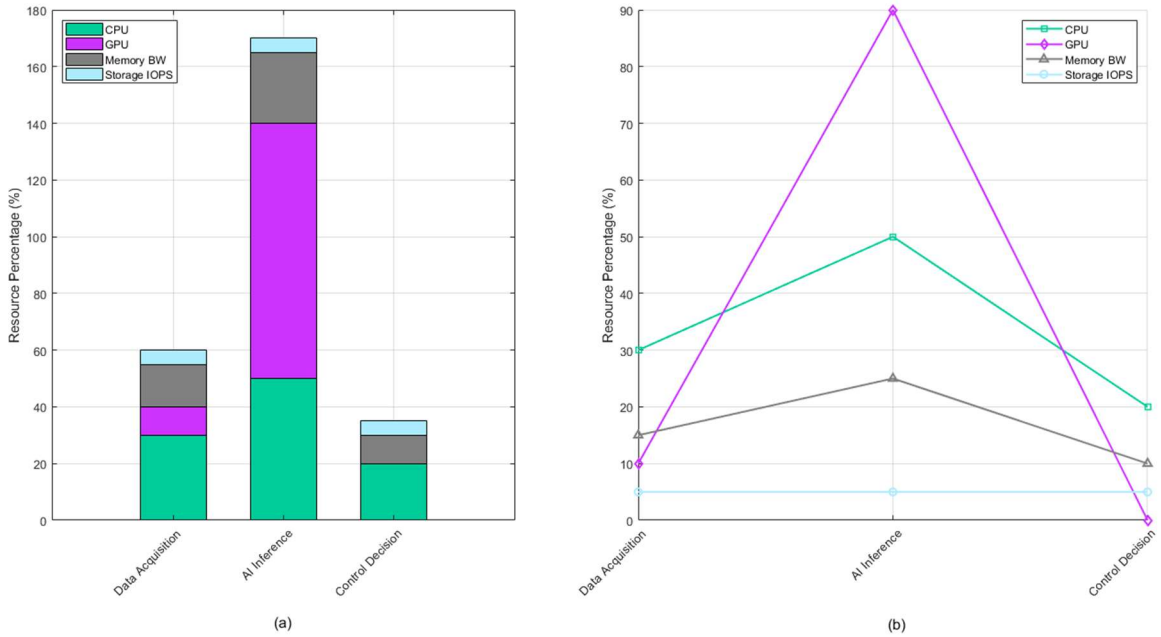

(a) Stacked resource allocation (b) Resource utilization curve

Figure 3: Analysis of resource allocation and utilization of edge computing nodes

Figure 3 shows the analysis of resource allocation and utilization of edge computing nodes. Among them, sub-graph (a) presents the multi-dimensional resource allocation of CPU, GPU, memory bandwidth, and storage IOPS (Input/Output Operations Per Second) in three microservices of data acquisition, AI inference, and control decision through stacked bar charts, reflecting the high dependence of AI inference on GPU resources and the balanced resource demand of control decision services. Sub-graph (b) compares the utilization distribution of each service on different resources in the form of a line chart, highlighting the dominant position of GPU resources in AI inference and the basic role of CPU resources in data acquisition. This directly reflects the resource scheduling strategy of IoT edge computing nodes in the scenario of smart grid distribution automation, and realizes the feasibility of efficient fault location and real-time control through containerized microservice architecture and dynamic resource allocation, which provides important support for improving the communication real-time and data processing capabilities of smart grids.

At the model acceleration level, TensorRT layer fusion technology is used to optimize the fault location algorithm. The transient current feature recognition model based on the improved ResNet-50 is converted into an FP16 precision engine, and the fault waveform data with a sampling rate of 4kHz/8kHz is adapted through a dynamic shape input mechanism. The model parallel inference framework is deployed, and the GPU streaming multiprocessor is used to realize the concurrent processing of multi-line fault features. The model compression rate is dynamically calculated by layer-by-layer weight norm:

$$C_r = 1 - \frac{\sum_{l=1}^{L} \left(\frac{1}{1+e^{-\lambda \cdot \| W_l \|_F}}\right)}{L} \tag{5}$$

The model parameters are dynamically compressed by the Sigmoid function of the layer-by-layer weight norm $\| W_l \|_F$. The algorithm dynamic loading framework is designed, and the OCI (open container initiative) standard algorithm warehouse management system is constructed. The control decision service interacts with the algorithm warehouse through the gRPC (Google Remote Procedure Call) interface, and the OCI image specification is used to implement the version control and dependency management of the algorithm container. The Kubernetes device plug-in mechanism is used to dynamically allocate GPU resources, and the process-level isolation of the algorithm container is implemented through the gVisor sandbox. The container image uses the distroless basic image, and the SSH (Secure Shell) service and interactive shell are disabled. The model federation update mechanism is developed, and the TensorFlow Federated client is deployed to implement differential privacy protection. A synchronization channel with the cloud training server is established through the OPC UA over TSN interface. The event triggering mechanism is used to implement the incremental update of model parameters. When the line impedance mutation exceeds the threshold, the model hot update process is triggered, and the business continuity of the algorithm iteration process is ensured through the version rollback mechanism. The differential privacy noise injection mechanism is:

$$\tilde{g}_t = g_t + \mathcal{N}(0, \sigma^2 \cdot \Delta_g^2) \tag{6}$$

Among them, $\sigma = \frac{\sqrt{2\ln(1.25/\delta)}}{\epsilon}$; Δg is the gradient sensitivity. The eBPF network traffic perception module is deployed to implement packet-level traffic feature extraction at the XDP layer. The transmission latency and jitter characteristics of GOOSE/SV messages are captured through the eBPF program to build a traffic profile for latency-sensitive services. The Prometheus monitoring system is integrated, and a custom Exporter is used to implement real-time collection of TSN network QoS parameters. The number of microservice instances is dynamically adjusted through the HPA (Horizontal Pod Autoscaler) strategy.

Security protection uses Intel SGX (Intel Software Guard Extensions) technology to build a trusted execution environment and encrypt the core computing process of the fault location algorithm in memory. A remote authentication service is deployed to verify the integrity of the algorithm container, and the SM9 national secret algorithm is used to implement identity-based encryption of control instructions. SGX Sealing is used to implement persistent storage of keys to ensure rapid reconstruction of the security environment after the device is restarted.

II. C.Digital Twin Modeling Method

The multi-physics coupling model of feeder automation devices is established based on the Modelica language, and the electromagnetic transient simulation kernel is constructed using the open source simulation platform OpenModelica. For the 10kV ring main unit devices, a refined model including vacuum circuit breaker, current transformer, and voltage transformer is established: the movement of the circuit breaker contact is described by the contact mechanics equation; the arc characteristics of the arc extinguishing chamber are characterized by the Mayr model; the transformer core saturation effect is modeled by the Jiles-Atherton hysteresis model. The functional mockup unit is exported through the FMI (Functional Mockup Interface) 2.0 standard to achieve interface integration with the digital twin platform. The parameter identification algorithm is deployed on the distribution

terminal device side, and the improved particle swarm optimization algorithm is used to realize model parameter calibration. The real-time operation data of the ring main unit (including the circuit breaker opening and closing coil current, contact travel curve, and busbar voltage distortion rate) is collected through the OPC UA interface to build a parameter estimation model for multi-dimensional state variables. The inertia weight factor is set to decrease nonlinearly with the number of iterations to optimize the convergence speed of the algorithm. The speed update equation of the PSO (Particle Swarm Optimization) algorithm is:

$$v_i^{t+1} = \omega \cdot v_i^t + c_1 r_1 (pbest_i - x_i^t) + c_2 r_2 (gbest - x_i^t) \tag{7}$$

Among them, ω is the inertia weight; c_1 and c_2 are learning factors; r_1 and r_2 are random numbers, and the model parameters are adjusted dynamically.

A real-time data interaction interface based on OPC UA is developed, and a hierarchical information model design is adopted. The top layer defines the object type of the feeder automation devices, including sub-objects such as circuit breaker state, protection signal, and electrical quantity measurement. The middle layer uses the address space optimization algorithm to map the IEC 61850 public data class to the OPC UA node structure. The bottom layer realizes deterministic transmission through the TSN network and adopts the publish-subscribe mechanism to ensure data synchronization latency. A closed-loop verification system of digital twins and physical devices is constructed, and an FPGA-based hardware-in-the-loop simulator is deployed on the ring main cabinet side. The electromagnetic transient calculation results of the digital twin model are output to the secondary circuit of the physical device through the digital-to-analog converter, and the device response signal is collected and fed back to the model. The dynamic time warping algorithm is used to align the timing data of the virtual and real systems, triggering the online correction mechanism of the model parameters.

A fault behavior prediction algorithm is developed for the single-phase grounding fault scenario of the distribution network. Fault currents with different transition resistances are injected into the digital twin model, and the electromagnetic field distribution during arc grounding is calculated by the finite element method. The LSTM (Long Short-Term Memory) network is used to establish the mapping relationship between fault characteristics and device status. The adversarial generative network is applied during the training process to enhance sample diversity. The control equation of the electromagnetic field distribution is:

$$\nabla \times (\nu \nabla \times \mathbf{A}) + \sigma \frac{\partial \mathbf{A}}{\partial t} = \mathbf{J}_s \tag{8}$$

Among them, ν is the magnetic resistivity; σ is the electrical conductivity; A is the magnetic vector potential; $\mathbf{J}_s$ is the source current density. The prediction results are pushed to the distribution master station in real-time through the OPC UA event notification service, and the joint loss function is designed as:

$$\mathcal{L}_{total} = \mathcal{L}_{LSTM} + \lambda \cdot (\mathbb{E}_{x \sim p_{data}}[\log D(x)] + \mathbb{E}_{z \sim p_z}[\log(1 - D(G(z))] \tag{9}$$

Combining the time series prediction loss $\mathcal{L}_{LSTM}$ and the adversarial loss, λ is the balance coefficient. The distributed collaborative computing architecture of the digital twin model is designed, and the model segmentation technology is used to decompose the electromagnetic transient computing task into the line section sub-model and the device-level sub-model. The line section sub-model is deployed in the cloud computing cluster, and parallel computing is used to accelerate large-scale power grid simulation. The device-level sub-model is deployed on the edge computing gateway and interacts with the physical device in real-time through the OPC UA over TSN interface. The consistent hashing algorithm is used to achieve dynamic load balancing of model sharding. To ensure the security of the digital twin system, the attribute-based access control (ABAC) strategy is used to manage the OPC UA interface permissions. Attribute dimensions such as device type, geographic location, and operation type are defined, and a multi-level access control policy library is established. In response to model parameter tampering attacks, lightweight blockchain nodes are deployed to store key operation logs and model version hash values on the chain.

Figure 4 shows the digital twin modeling and virtual-real interaction system architecture. Combining the theme of the integration of smart grid and IoT technology, the collaborative working mechanism of physical devices, communication network, digital twin model, and application system in distribution automation is reflected. The physical layer collects real-time data of devices such as ring network cabinets through sensor networks and hardware-in-the-loop simulators, and interacts with the digital twin layer in a closed-loop. The communication layer relies on TSN network and OPC UA interface to achieve low-latency, high-reliability data transmission and synchronization. The digital twin layer uses multi-physics field coupling model (electromagnetic transient, mechanical motion, and thermodynamic model) combined with AI algorithm to complete parameter identification, fault prediction, and distributed computing. The application layer realizes a complete business closed-loop from real-time monitoring to self-healing control, and at the same time ensures the reliability and safety of system operation through security protection mechanism, thereby comprehensively improving the real-time perception, dynamic optimization, and autonomous decision capabilities of smart grids.

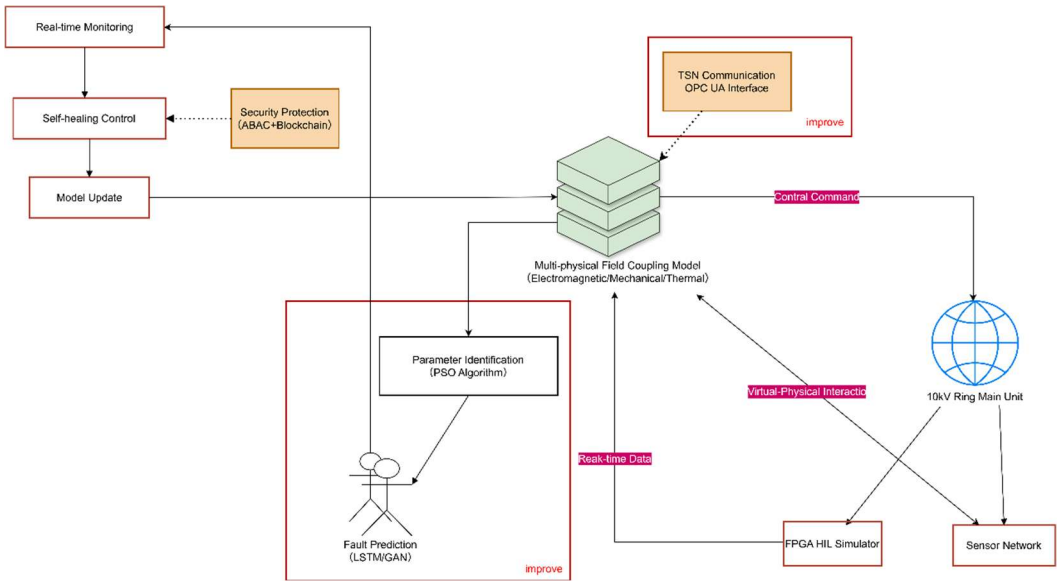

Figure 4: Digital twin modeling and virtual-real interaction system architecture

II. D.Distribution Automation Performance Verification System

This study constructs a multi-dimensional verification framework, deploys network analyzers and embedded timestamps using distributed test nodes, and calculates end-to-end communication latency through hardware timestamp differences. A periodic traffic injection experiment is designed, and Spirent TestCenter is used to simulate multi-service traffic to verify the TSN scheduling mechanism. Fault handling verification uses a dual-track comparison test to simulate faults on the electromagnetic transient simulation platform and the physical ring network cabinet. The positioning accuracy is compared by loading the algorithm with the TensorRT inference engine, and the self-healing recovery time is calibrated based on the IEC 61850 event sequence record. Cloud-edge collaborative testing builds a three-level stress model and simulates dynamic migration of algorithm containers through Kubernetes clusters. Heartbeat packets are used to detect the success rate of task offloading, and the Helm tool is combined to verify the model update frequency. An attack and defense confrontation framework is deployed for security verification, and a nationally certified cryptographic machine is used to test encryption performance. A multi-type attack traffic library is built to verify the intrusion detection model. Through the red-blue confrontation drill, the MACsec anti-replay attack capability is tested, and the electromagnetic protection effect of the physical layer is monitored using a spectrum analyzer. The test tool chain integrates modular devices to achieve multi-parameter synchronous acquisition, and the boundary scan link is designed according to IEEE standards to ensure full-stack coverage.

III. Experimental Test

III. A. Experimental Design

This study uses a multi-source heterogeneous dataset, covering PMU measurement data, device status parameters, user power consumption information, and electromagnetic transient simulation data. The ring main unit operation data is collected in real-time through the OPC UA interface, and the digital twin model built by Modelica is used to generate fault scenario samples. The dataset is divided into training set, validation set, and test set in a ratio of 8:1:1. Among them, the training set is used for model parameter optimization; the validation set is used for algorithm hyperparameter tuning; the test set is used for multi-model performance comparison. Real-time data is incrementally updated under differential privacy protection through the federated learning framework. The simulation data uses the FMI 2.0 standard to perform closed-loop verification with physical devices, and the dynamic time warping algorithm is used to align the virtual and real system time series data. The experimental environment deploys an improved 5G-TSN communication architecture, an edge computing gateway cluster, and a digital twin verification platform to test the performance differences between the Modelica digital twin model, the LSTM-GAN (Long Short-Term Memory-Generative adversarial network) fault prediction model, the ResNet-50 transient current identification model, the DBSCAN (Density-Based Spatial Clustering of Applications with Noise) fault location model, and the improved 5G-TSN model in terms of latency, fault handling, cloud-edge collaboration, and security.

III. B. Communication and Computing Performance Testing

This section builds a multi-dimensional evaluation system to verify the comprehensive performance of the improved 5G-TSN model from three dimensions: latency (communication layer), edge inference efficiency (computing layer), and cloud-edge data consistency (collaboration layer).

Its latency characteristics are analyzed through multi-scenario comparative experiments. The test covers five typical scenarios: normal load, traffic surge, wide area synchronization, encrypted transmission, and multi-service concurrency, and is carried out from three dimensions: end-to-end latency, communication latency, and processing latency. The experiment compares the performance differences between the improved 5G-TSN model and the Modelica, LSTM-GAN, ResNet-50, and DBSCAN models, and evaluates their latency performance in different business scenarios.

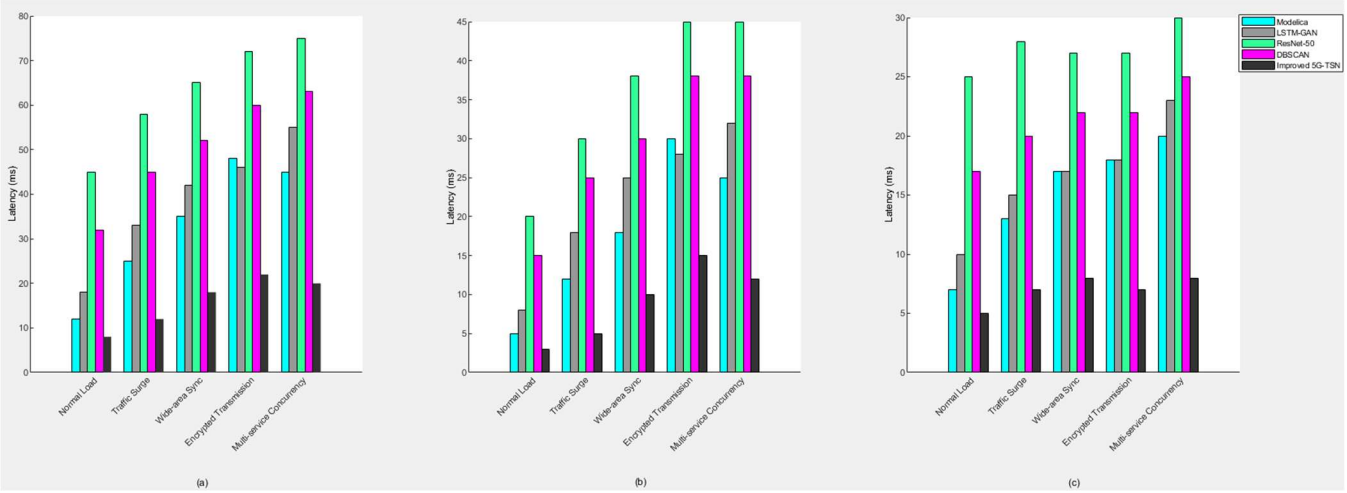

(a) End-to-end latency (b) Communication latency (c) Processing latency

Figure 5: Comparison of latency performance of various models in multiple scenarios

Figure 5 shows the latency performance test results of different models and four models: Modelica, LSTM-GAN, ResNet-50, and DBSCAN in five typical scenarios (normal load, traffic surge, wide area synchronization, encrypted transmission, and multi-service concurrency). The horizontal axis represents the five scenarios, and the vertical axis is the latency index (unit: ms), including three sub-graphs: end-to-end latency, communication latency, and processing latency. From the data, the improved 5G-TSN model performs well in most scenarios, and its end-to-end latency in the normal load scenario is only about 8ms. In the encrypted transmission scenario, its end-to-end latency increases to about 22ms. This differentiated data reflects the trade-offs between different models in resource allocation, hardware acceleration, and encryption overhead.

The reasons behind the data in Figure 5 are closely related to the underlying mechanisms of each model. The improved 5G-TSN model implements hard-isolated network slicing and dynamic bandwidth adjustment through the FlexE interface, significantly reducing latency in normal load and traffic surge scenarios, and increasing communication latency in traffic surge scenarios. However, in encrypted transmission scenarios, the improved 5G-TSN increases communication latency due to the activation of the AES-256-GCM encryption algorithm, but its processing latency remains low, thanks to the optimization of encryption tasks by the hardware acceleration unit. In addition, ResNet-50 and improved DBSCAN show high latency when processing complex computing tasks, reflecting the limitations of traditional AI models in resource-constrained environments. These data show that the improved 5G-TSN model achieves overall performance optimization through the deep integration of time-sensitive networks and edge computing, but security and real-time performance need to be further balanced in encryption scenarios.

To evaluate the inference performance of different models in edge computing environments, the inference efficiency of Modelica, LSTM-GAN, ResNet-50, DBSCAN, and improved 5G-TSN models is tested experimentally. The experiment deploys each model on the embedded edge gateway, focusing on monitoring the core indicators of inference latency, model volume, accuracy, and energy consumption, and verifies the optimization effect of the model in terms of lightweight and real-time performance.

Table 2: Comparison of edge inference efficiency

Model	Average Inference Latency (ms)	Model Size (MB)	Accuracy (%)	Power Consumption (W)
Modelica	45.6	1520	82.3	18.5
LSTM-GAN	32.1	890	91.7	15.2
ResNet-50	58.4	98	93.5	22.8
DBSCAN	24.9	12	88.6	9.7
Improved 5G-TSN	5.8	0.8	94.1	6.3

Table 2 shows the comparison of edge inference efficiency between the improved 5G-TSN model and four models, Modelica, LSTM-GAN, ResNet-50, and DBSCAN, including four key indicators: average inference latency, model size, accuracy, and power consumption. The improved 5G-TSN model shows obvious advantages in various performances, with an average inference latency of only 5.8ms, much lower than other models, including 45.6ms for Modelica and 58.4ms for ResNet-50. In terms of model size, the improved 5G-TSN significantly outperforms the other models, especially Modelica (1520MB), with a parameter size of 0.8MB, reflecting its lightweight design. In terms of accuracy, the improved 5G-TSN reaches 94.1%, slightly higher than ResNet-50's 93.5% and significantly ahead of DBSCAN (88.6%) and Modelica (82.3%). In terms of power consumption, the 6.3W of the improved 5G-TSN is also better than other models, especially the ResNet-50 (22.8W) and Modelica (18.5W) with higher power consumption, showing its outstanding performance in energy efficiency.

Behind these performance advantages is the design concept of the improved 5G-TSN model based on the deep integration of IoT technology and 5G-TSN. Through the FlexE interface to achieve hard-isolated network slicing, combined with the TSN time synchronization protocol, the model effectively reduces communication latency and compresses the model volume through the lightweight ST-GCN algorithm, while using the TensorRT optimization engine to improve the inference speed and accuracy. In contrast, Modelica relies on complex electromagnetic transient simulation, resulting in high latency and large model volume; although ResNet-50 has a high accuracy rate, its deep learning structure makes it consume too much power when running on edge devices; DBSCAN, as a traditional clustering algorithm, has fast inference speed and low power consumption, but its accuracy is limited. Due to the complexity of the generative adversarial network, LSTM-GAN performs generally in terms of model volume and inference latency.

Through three-dimensional surface analysis, the correlation between task migration success rate, resource utilization, and coordination latency is quantified. The three-level pressure model is constructed experimentally to simulate the dynamic migration process of algorithm containers. The task offloading success rate is detected through heartbeat packets, and the model update frequency is verified in combination with the Helm tool. The cloud-edge coordination performance of the improved 5G-TSN model and different models is compared.

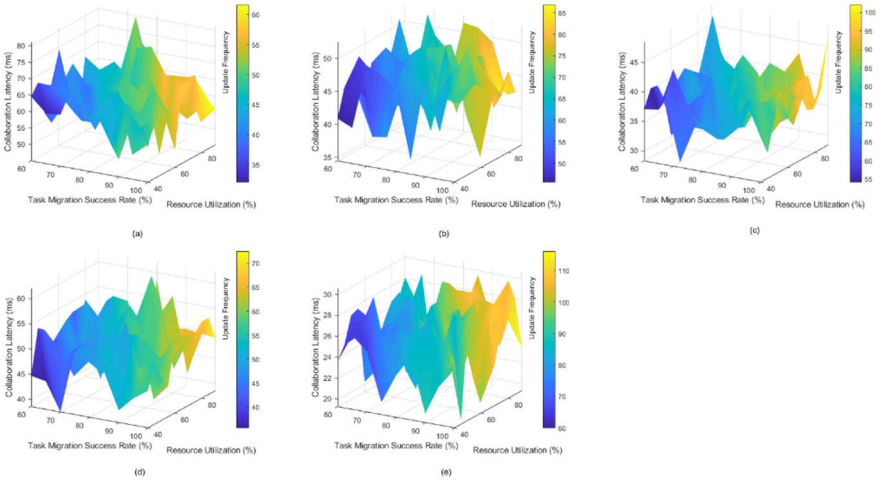

(a) Modelica (b) LSTM-GAN (c) ResNet-50

(d) DBSCAN (e) Improved 5G-TSN

Figure 6: 3D surface analysis of cloud-edge collaboration capability

Figure 6 shows the 3D surface data of different models in the cloud-edge collaboration capability test through five sub-graphs. The horizontal axis represents the task migration success rate (60%-100%); the vertical axis represents the resource utilization rate (40%-90%); the Z axis reflects the collaboration latency (ms). From the data, Modelica shows a higher latency (Z≈60-70ms) under high resource utilization, while improved 5G-TSN achieves a lower latency (Z≈20-28ms) under the same conditions, indicating that the model is more adaptable to parameter changes. The color mapping further reveals the difference in model update frequency. Warmer colors indicate higher update frequency, and colder colors indicate lower update frequency.

Behind these data, the underlying mechanism differences of each model in cloud-edge collaboration are reflected. The improved 5G-TSN model optimizes task migration and resource allocation through dynamic bandwidth adjustment algorithm and TSN gating mechanism, thereby significantly reducing latency and increasing update frequency; in contrast, the Modelica model relies on complex physical simulation calculations, resulting in high latency and limited update frequency. Overall, the data in Figure 6 not only verifies the superiority of the improved 5G-TSN model in cloud-edge collaboration, but also reveals the applicability and limitations of other models in specific scenarios, providing an important reference for the integration of smart grid and IoT technology.

III. C. Comprehensive Fault Handling Test

Aiming at the core requirement of the distribution automation system, that is, the ability to respond to faults quickly, this section compares the positioning accuracy of different models in five fault scenarios: single-phase grounding, phase-to-phase short circuit, line break, arc, and compound fault. The experiment simulates faults synchronously through the electromagnetic transient simulation platform and the physical ring network cabinet to test the differences in fault location accuracy of each model.

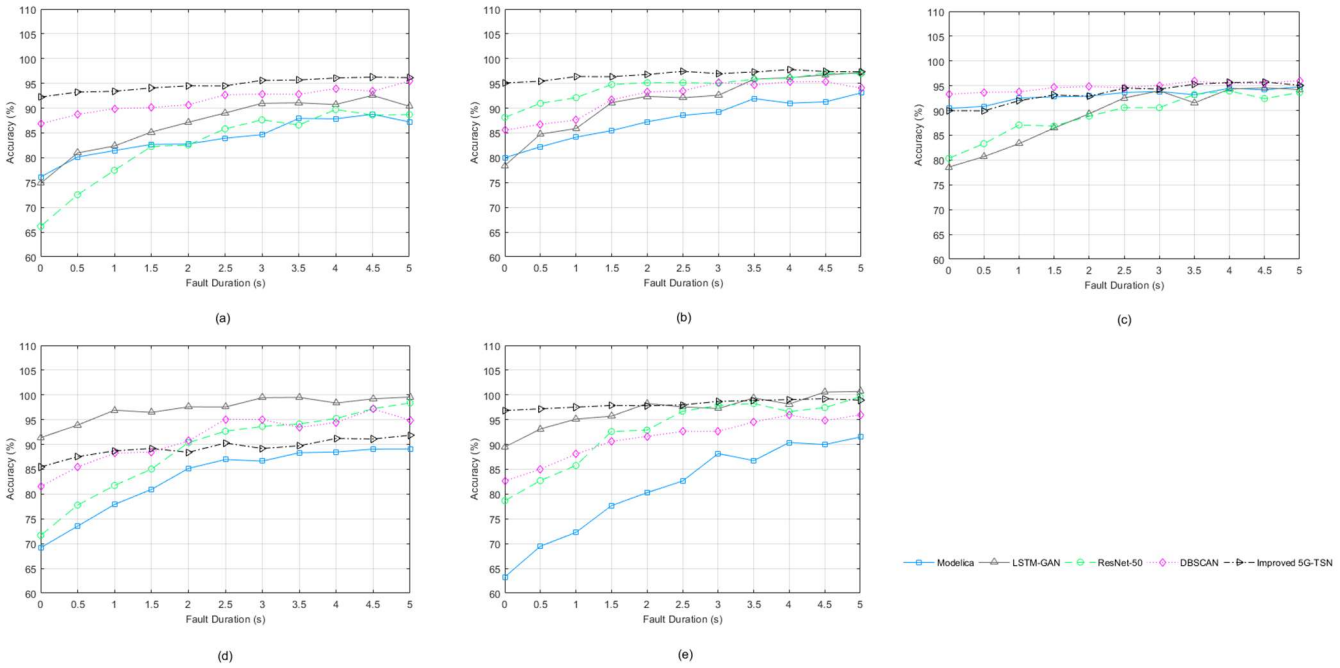

(a) Single-phase ground fault (b) Phase-to-phase short circuit fault (c) Line break fault

(d) Arc fault (e) Compound fault

Figure 7: Comparison of model performance under five fault scenarios

Figure 7 shows the performance comparison of different models under five typical fault scenarios. The horizontal axis represents the fault duration (0 to 5 seconds), and the vertical axis represents the fault location accuracy. From the data comparison, the improved 5G-TSN model shows significant advantages in most scenarios. In (a), its accuracy reaches more than 95% within 3 seconds and remains stable. In (e), the model quickly increases to about 96% within 2 seconds, showing its superiority in complex scenarios. However, in scenario (d), the performance of the improved 5G-TSN model is relatively insufficient, only maintaining at about 85%-92%, reflecting its limitations in high electromagnetic interference environments.

The data in Figure 7 reflects the differences in model design and underlying mechanisms, as well as their adaptability to different types of faults. The improved 5G-TSN model realizes hard-isolated network slicing by integrating FlexE interfaces and optimizes the transmission of latency-sensitive service flows in combination with TSN technology, so that it can respond quickly and maintain high accuracy in most scenarios. However, in arc faults, due to the impact of electromagnetic interference on communication links, its mechanism based on the time synchronization protocol is subject to certain limitations, resulting in slightly inferior performance to the LSTM-GAN model, which enhances the learning ability of complex fault features through adversarial generative networks. ResNet-50, on the other hand, demonstrates the advantages of convolutional neural networks in image data processing in scenarios with obvious features such as phase-to-phase short circuits. These results show that the performance differences of different models are closely related to their technical characteristics and also verify the practical application potential of the integration of smart grid and IoT technologies in distribution automation.

Table 3: Comparison of resource consumption of cloud-edge collaborative task migration

Model	CPU Peak Usage Rate (%)	Peak Memory Usage (MB)	Bandwidth Fluctuation Range (Mbps)	Task Migration Time (ms)	Resource Recovery Efficiency (%)
Improved 5G-TSN	62.3	980	75-88	18.2	94.5
Modelica	78.6	1520	110-130	42.7	81.2
LSTM-GAN	71.5	1350	90-105	33.1	87.3
ResNet-50	85.4	1890	120-140	49.8	76.8
DBSCAN	67.9	1120	80-95	27.4	89.1

Table 3 shows the resource consumption and efficiency comparison of different models in the process of cloud-edge collaborative task migration, covering five key dimensions: CPU peak utilization, memory usage, bandwidth fluctuation range, migration time, and resource recovery efficiency. From the data, the improved 5G-TSN model performs well in multiple indicators. Its CPU peak utilization is 62.3%, significantly lower than ResNet-50's 85.4% and Modelica's 78.6%; its memory usage is 980MB, much lower than Modelica's 1520MB and ResNet-50's 1890MB. In addition, the bandwidth fluctuation range of the improved 5G-TSN model is 75-88Mbps, and the migration task takes only 18.2ms, both of which are better than other models, and its resource recovery efficiency is as high as 94.5%, far exceeding Modelica's 81.2% and ResNet-50's 76.8%. In contrast, ResNet-50 has the largest resource overhead due to its reliance on GPU inference, while Modelica has a low resource recovery efficiency due to complex simulation calculations.

The differences in these data reflect the differences in the design mechanisms and applicable scenarios of each model. The improved 5G-TSN model optimizes task migration and resource allocation through dynamic bandwidth adjustment algorithm and TSN gating mechanism, thereby significantly reducing latency. For example, the excellent performance in bandwidth fluctuation range and migration time is due to the hard isolation network slice design and time synchronization protocol support of the FlexE interface. However, the Modelica model relies on complex physical simulation calculations, resulting in low resource recovery efficiency and long migration time (42.7ms). The high CPU and memory usage of the ResNet-50 model is mainly due to its high dependence on deep learning inference, which makes it perform poorly in resource-constrained environments. Although the LSTM-GAN and DBSCAN models perform relatively evenly in some scenarios, they are insufficient in resource recovery efficiency (87.3% and 89.1%, respectively). These results further verify the comprehensive advantages of the improved 5G-TSN model in the scenario of the integration of smart grid and IoT technology.

III. D. Security Test

Security is the cornerstone of the integration of smart grid and IoT. This section constructs a radar chart evaluation system from five dimensions: encryption performance, intrusion detection rate, anti-replay attack, data integrity, and privacy protection. The experiment deploys an attack and defense framework, uses a nationally certified cryptographic machine to test encryption performance, and builds a multi-type attack traffic library to verify the intrusion detection model. The MACsec anti-replay attack capability is tested through a red-blue confrontation exercise, and the security protection level of each model is comprehensively compared.

(a) Modelica (b) LSTM-GAN (c) ResNet-50

(d) DBSCAN (e) Improved 5G-TSN

Figure 8: Security test radar chart

Figure 8 shows the performance of the five models in the security test, presenting the comparison of five dimensions in the form of radar charts: encryption performance, intrusion detection rate, anti-replay attack, data integrity, and privacy protection. Each sub-graph represents a model, with a numerical range of 0 to 100 points. Among them, the improved 5G-TSN model performs well in all dimensions, especially in encryption performance (98 points) and privacy protection (96 points). Overall, the DBSCAN model has the highest score in the anti-replay attack dimension (95 points); the ResNet-50 transient current identification model performs well in data integrity (95 points), but is slightly insufficient in privacy protection (75 points). These data show that different models have different focuses on security, and the improved 5G-TSN model has the best comprehensive performance.

Behind these data differences, it reflects the differences in the design mechanisms and applicable scenarios of each model. For example, the improved 5G-TSN model effectively improves encryption performance and privacy protection capabilities through the dual isolation mechanism of FlexE interface and IPSec tunnel, combined with the AES-256-GCM encryption algorithm. The Modelica digital twin model relies on high-precision electromagnetic transient modeling and real-time data interaction to ensure a high level of data integrity. The LSTM-GAN model uses adversarial generative networks to enhance sample diversity, thereby improving the intrusion detection accuracy. The improved DBSCAN model performs well in anti-replay attack scenarios through an optimized fault location algorithm. In addition, the ResNet-50 transient current identification model performs well in data integrity with the help of GPU acceleration and deep learning inference framework, but its emphasis on privacy protection is low, resulting in a low score in this dimension. Overall, the differences in security of these models are due to the targeted design of their technical architecture and application scenarios, and also reflect the complexity of multi-dimensional security requirements in the process of integrating smart grid and IoT technologies.

IV. Application Prospects

IV. A. Technology Promotion Path

For rural power grid transformation scenarios, it is necessary to focus on breaking through the communication coverage blind spots and low device operation and maintenance efficiency caused by high altitude and

mountainous terrain. By deploying LoRaWAN/ZigBee dual-mode heterogeneous sensor networks and combining the cross-standard multi-protocol adaptation capabilities of the FlexE interface, millisecond-level acquisition and transmission of device status parameters (contact stroke, partial discharge) of old ring network cabinets can be achieved. The TSN switch IEEE 802.1Qbv gating mechanism is used to optimize the telemetry data transmission timing of the feeder terminal unit, and the device status parameter modeling standards are unified through the OPC UA information model to reduce the cost of operation and maintenance data governance.

In the multi-energy complementary system of the industrial park, it is necessary to solve the bottleneck of dynamic collaborative control of distributed photovoltaic, energy storage clusters, and charging pile loads. Based on the containerized microservice architecture, a lightweight spatiotemporal graph convolutional network is deployed, and edge computing gateway resources with AI inference capabilities are dynamically scheduled through Kubernetes to achieve park-level source-grid-load-storage collaborative optimization. Combined with the improved 5G-TSN hybrid scheduling algorithm, the efficiency of dynamic bandwidth adjustment is improved. The Modelica electromagnetic transient model and LSTM-GAN fault prediction module are integrated through the digital twin platform to support the improvement of single-phase grounding fault location accuracy and power supply restoration time compression, and adapt to the millisecond-level charging and discharging switching of electrochemical energy storage and the real-time response needs of electric vehicle load aggregators.

IV. B. Economic Evaluation

Compared with the architecture of traditional SCADA systems that rely on fiber-optic communication and centralized cloud computing, the technical solution proposed in this study that integrates the Internet of Things and the improved 5G-TSN model presents differentiated advantages in terms of life cycle costs. Traditional architectures require large-scale deployment of fiber-optic networks to meet real-time requirements, resulting in initial capital expenditures concentrated on communication infrastructure construction, and additional investment in multi-protocol conversion devices and distributed storage units due to data island problems, significantly increasing operation and maintenance costs. This solution uses the FlexE interface to hard-isolate network slices and TSN gating mechanisms to achieve dynamic bandwidth allocation for multi-service traffic, while reducing fiber dependence and improving communication resource utilization; combined with containerized microservice architecture and edge computing node deployment, the focus of data governance is moved forward to the perception layer, reducing the computing power consumption of cloud data cleaning and model iteration, thereby compressing long-term operation and maintenance expenses.

In terms of scalability costs, traditional SCADA systems need to be transformed at the architectural level for distributed energy access scenarios due to protocol heterogeneity and centralized processing bottlenecks, involving secondary investment and business interruption risks. This solution unifies the modeling standards of device status parameters through the OPC UA information model, and implements elastic scaling of microservices based on Kubernetes, supporting rapid functional iteration of source-grid-load-storage collaborative control scenarios. In addition, the integration of the digital twin platform and the federated learning framework enables the fault prediction model to replace the full algorithm replacement of the traditional SCADA (Supervisory Control And Data Acquisition) system through incremental updates, reducing the marginal cost of technology upgrades. From a full life cycle perspective, the initial hardware investment of this fusion architecture is slightly higher than that of traditional solutions, but by increasing resource reuse and compressing operation and maintenance complexity, it can achieve convergence and overtaking of TCO (Total cost of ownership) within a 3-5 year cycle.

IV. C. Future Expansion Direction

The terahertz frequency band and intelligent metasurface technology for 6G communication can further enhance the dynamic coverage capability of the distribution automation system. By applying the channel state prediction mechanism of the AI native architecture, real-time compensation of multipath effects and electromagnetic interference in the submillimeter wave frequency band can be achieved, supporting the deterministic communication needs of feeder terminal units in complex electromagnetic environments. Combining network slicing and distributed AI decision, a control plane with end-to-end latency less than 1ms is constructed to adapt to the rapid topology reconstruction and collaborative control needs in scenarios with high penetration of distributed energy.

The quantum key distribution protocol and post-quantum encryption algorithm of quantum communication technology can provide a physical layer security enhancement solution for distribution automation. The synchronization mechanism based on quantum entanglement can improve the time synchronization accuracy of the wide-area monitoring system to the picosecond level, and at the same time realize the anti-interference transmission of control instructions through quantum teleportation. Combined with the federated learning

framework of edge computing nodes, a collaborative verification system of quantum secure communication and classical power business is constructed to provide a protection basis for new power systems against quantum computing attacks.

V. Conclusions

This paper focuses on the integration of smart grid and Internet of Things technology, and proposes a technical solution based on an improved 5G-TSN model. Combining the ubiquitous perception and edge computing capabilities of the Internet of Things, it realizes real-time control and efficient data processing of the distribution automation system. By building a multi-dimensional sensor network, deploying edge computing gateways, and digital twin modeling, the communication real-time performance, fault response speed, and intelligence level of the distribution system are effectively improved. The research provides a technical support for highly elastic and adaptive new power systems, and demonstrates its broad application prospects in rural power grid transformation, industrial park energy management, and other scenarios. In the future, the deep integration of this architecture with 6G communication and quantum encryption technology can be further explored to promote the development of the power system in a more efficient and secure direction.

References

[1] Kulkarni V, Sahoo S K, Thanikanti S B, et al. Power systems automation, communication, and information technologies for smart grid: A technical aspects review[J]. TELKOMNIKA (Telecommunication Computing Electronics and Control), 2021, 19(3): 1017-1029.

[2] Omitaomu O A, Niu H. Artificial intelligence techniques in smart grid: A survey[J]. Smart Cities, 2021, 4(2): 548-568.

[3] Kang C, Kirschen D, Green T C. The evolution of smart grids[J]. Proceedings of the IEEE, 2023, 111(7): 691-693.

[4] Medina C, Ana C R M, González G. Transmission grids to foster high penetration of large-scale variable renewable energy sources–A review of challenges, problems, and solutions[J]. International Journal of Renewable Energy Research (IJRER), 2022, 12(1): 146-169.

[5] Melodi A O. Customer-oriented power supply reliability and evaluation for Nigeria's electricity supply industry[J]. Electrical Engineering, 2024, 106(3): 2209-2217.

[6] Kojima H, Nagasawa K, Todoroki N, et al. Influence of renewable energy power fluctuations on water electrolysis for green hydrogen production[J]. international journal of hydrogen energy, 2023, 48(12): 4572-4593.

[7] Vaithianathan M, Patil M, Ng S F, et al. Comparative study of FPGA and GPU for high-performance computing and AI[J]. ESP International Journal of Advancements in Computational Technology (ESP-IJACT), 2023, 1(1): 37-46.

[8] Kermani M, Shirdare E, Parise G, et al. A comprehensive technoeconomic solution for demand control in ports: Energy storage systems integration[J]. IEEE Transactions on Industry Applications, 2022, 58(2): 1592-1601.

[9] Li J, Gu C, Xiang Y, et al. Edge-cloud computing systems for smart grid: state-of-the-art, architecture, and applications[J]. Journal of Modern Power Systems and Clean Energy, 2022, 10(4): 805-817.

[10] Brosinsky C, Naglič M, Lehnhoff S, et al. A Fortunate Decision That You Can Trust: Digital Twins as Enablers for the Next Generation of Energy Management Systems and Sophisticated Operator Assistance Systems[J]. IEEE Power and Energy Magazine, 2024, 22(1): 24-34.

[11] Sriram G S. Resolving security and data concerns in cloud computing by utilizing a decentralized cloud computing option[J]. International Research Journal of Modernization in Engineering Technology and Science, 2022, 4(1): 1269-1273.

[12] Arefifar S A, Alam M S, Hamadi A. A review on self-healing in modern power distribution systems[J]. Journal of Modern Power Systems and Clean Energy, 2023, 11(6): 1719-1733.

[13] Hashmi S A, Ali C F, Zafar S. Internet of things and cloud computing ‐ based energy management system for demand side management in smart grid[J]. International Journal of Energy Research, 2021, 45(1): 1007-1022.

[14] Yuan D, Bhardwaj A, Petersen I, et al. Towards online optimization for power grids[J]. ACM SIGENERGY Energy Informatics Review, 2021, 1(1): 51-58.

[15] Butt O M, Zulqarnain M, Butt T M. Recent advancement in smart grid technology: Future prospects in the electrical power network[J]. Ain Shams Engineering Journal, 2021, 12(1): 687-695.

[16] Yang W, Du H, Liew Z Q, et al. Semantic communications for future internet: Fundamentals, applications, and challenges[J]. IEEE Communications Surveys & Tutorials, 2022, 25(1): 213-250.

[17] Kusumawati R. Integrating big data analytics into supply chain management: Overcoming data silos to improve real-time decision-making[J]. International Journal of Advanced Computational Methodologies and Emerging Technologies, 2025, 15(2): 17-26.

[18] Cao Y, Xiao S, Ye Z, et al. Analysis and suppression of operational overvoltage and inrush current for high ‐ speed trains by automatic phase ‐ switching technique[J]. High Voltage, 2024, 9(3): 733-748.

[19] Ganivada P K, Jena P. A fault location identification technique for active distribution system[J]. IEEE Transactions on Industrial Informatics, 2021, 18(5): 3000-3010.

[20] Zhang W, Chang Z, Zhang C, et al. A quick fault location and isolation method for distribution network based on adaptive reclosing[J]. IET Generation, Transmission & Distribution, 2022, 16(4): 715-723.

[21] Hou J, Song G, Fan Y. Fault identification scheme for protection and adaptive reclosing in a hybrid multi-terminal HVDC system[J]. Protection and Control of Modern Power Systems, 2023, 8(2): 1-17.

[22] Ghiasi M, Wang Z, Mehrandezh M, et al. Evolution of smart grids towards the Internet of energy: Concept and essential components for deep decarbonisation[J]. IET Smart Grid, 2023, 6(1): 86-102.

[23] Hua H, Qin Z, Dong N, et al. Data-driven dynamical control for bottom-up energy Internet system[J]. IEEE Transactions on Sustainable Energy, 2021, 13(1): 315-327.

[24] Zhuang Y, Liu F, Huang Y, et al. A multiport DC solid-state transformer for MVDC integration interface of multiple distributed energy sources and DC loads in distribution network[J]. IEEE Transactions on Power Electronics, 2021, 37(2): 2283-2296.

[25] Orlando M, Estebsari A, Pons E, et al. A smart meter infrastructure for smart grid IoT applications[J]. IEEE Internet of Things Journal, 2021, 9(14): 12529-12541.
[26] Huang C, Sun C C, Duan N, et al. Smart meter pinging and reading through AMI two-way communication networks to monitor grid edge devices and DERs[J]. IEEE Transactions on Smart Grid, 2021, 13(5): 4144-4153.
[27] Yan Qunmin, Dong Xinzhou, Mu Jiahao, et al. Optimal configuration of active distribution network energy storage based on improved multi-objective particle swarm optimization algorithm[J]. Power System Protection and Control, 2022, 50(10): 11-19.
[28] Yang N, Han L, Liu R, et al. Multiobjective intelligent energy management for hybrid electric vehicles based on multiagent reinforcement learning[J]. IEEE Transactions on Transportation Electrification, 2023, 9(3): 4294-4305.
[29] Gueye T, Wang Y, Rehman M, et al. A novel method to detect cyber-attacks in IoT/IIoT devices on the modbus protocol using deep learning[J]. Cluster Computing, 2023, 26(5): 2947-2973.
[30] Sheba M A, Mansour D E A, Abbasy N H. A new low‐cost and low‐power industrial internet of things infrastructure for effective integration of distributed and isolated systems with smart grids[J]. IET Generation, Transmission & Distribution, 2023, 17(20): 4554-4573.
[31] Purnomo W, Candra W A, Manuel G M. Design of Remote Monitoring Application on Non-Rechargeable Battery Redundant System[J]. MOTIVECTION: Journal of Mechanical, Electrical and Industrial Engineering, 2023, 5(3): 447-460.
[32] Zhou B, Zou J, Chung C Y, et al. Multi-microgrid energy management systems: Architecture, communication, and scheduling strategies[J]. Journal of Modern Power Systems and Clean Energy, 2021, 9(3): 463-476.
[33] Shi M, Wang H, Xie P, et al. Distributed energy scheduling for integrated energy system clusters with peer-to-peer energy transaction[J]. IEEE Transactions on Smart Grid, 2022, 14(1): 142-156.